mTOR-Mediated Dedifferentiation of the Retinal Pigment Epithelium Initiates Photoreceptor Degeneration in Mice

Supplemental Figures 1-5

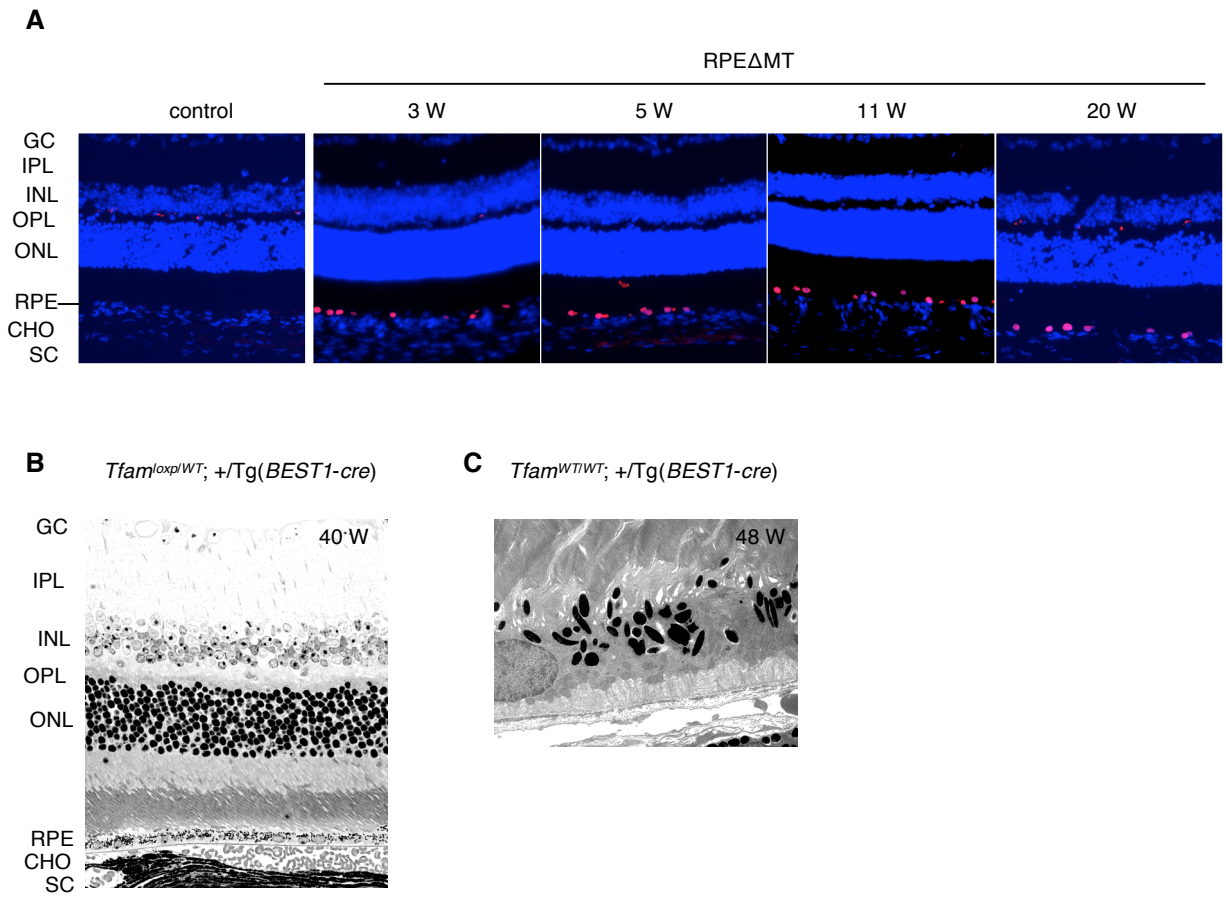

Figure S1. RPE-specific cre expression in RPEΔMT mice and absence of cre toxicity in controls. (**A**) Retinal frozen sections from albino RPEΔMT mice and a control were immunostained for cre (red). Control refers to *Tfam*$^{loxp/loxp}$ mice hereafter, unless otherwise stated. RPE-specific cre expression was observed at all ages tested. Background signals arising from the anti-mouse secondary antibody alone were occasionally seen in the SC and OPL layers. (**B**) A representative light micrograph of a retinal section from a 40-week-old *Tfam*$^{loxp/WT}$; +/Tg(*BEST1-cre)* mouse shows no abnormalities in any layer. (**C**) *Tfam*$^{WT/WT}$; +/Tg(*BEST1-cre*) mice have normal RPE ultrastructure at 48 weeks of age. Abbreviation: GC, ganglion cells layer; IPL, inner plexiform layer; INL, inner nuclear layer; OPL, outer plexiform layer; ONL, outer nuclear layer; RPE, retinal pigment epithelium; SC, sclera.

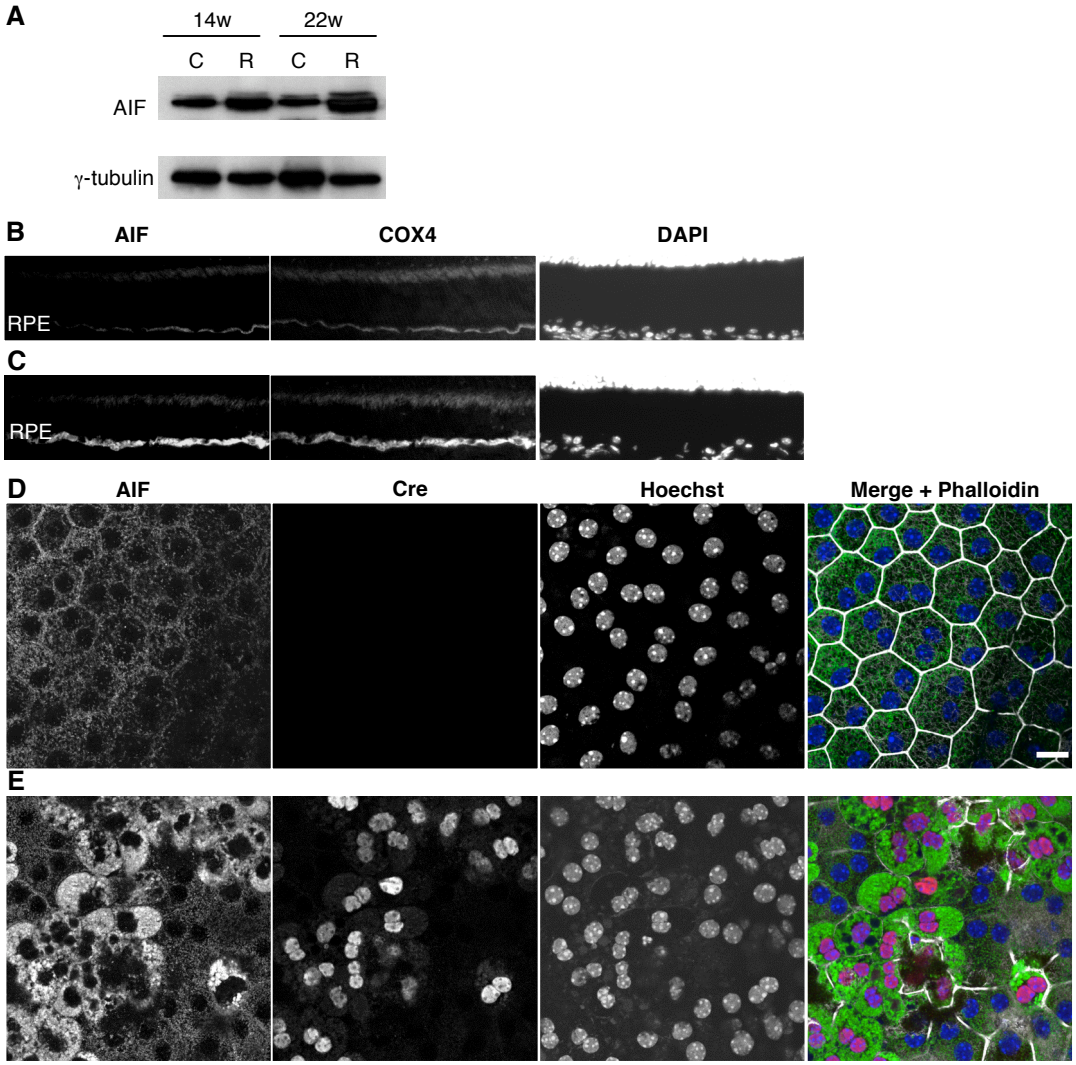

Figure S2. Effect of *Tfam* deficiency on RPE mitochondrial proteins and viability. (**A**) Immunoblot detects significantly increased AIF in isolated RPE cells from pigmented RPEΔMT mice (R) at 14 weeks and 22 weeks, compared to controls (C). (**B** and **C**) AIF and COX4 co-staining of retinal frozen sections shows increased reactivity of both proteins in an 18-week-old albino RPEΔMT mouse (**C**), compared to a control (**B**). (**D** and **E**) Confocal pictures of flatmounts stained for AIF and cre in albino RPEΔMT (**E**) and control (**D**) mice at 18 weeks. Phalloidin staining (default as white) was added at the end into merged pictures (green for AIF; red for cre; blue for Hoechst). AIF reactivity is clearly increased in the cytoplasm of cre-expressing RPE cells; however, nuclear translocation of AIF is not detected (**E)** because no nucleus turns white in the merged image. Nuclear condensation and DNA fragmentation are not remarkable in RPEΔMT RPE (Hoechst stain in panel **E**). Scale bar: 15 μm.

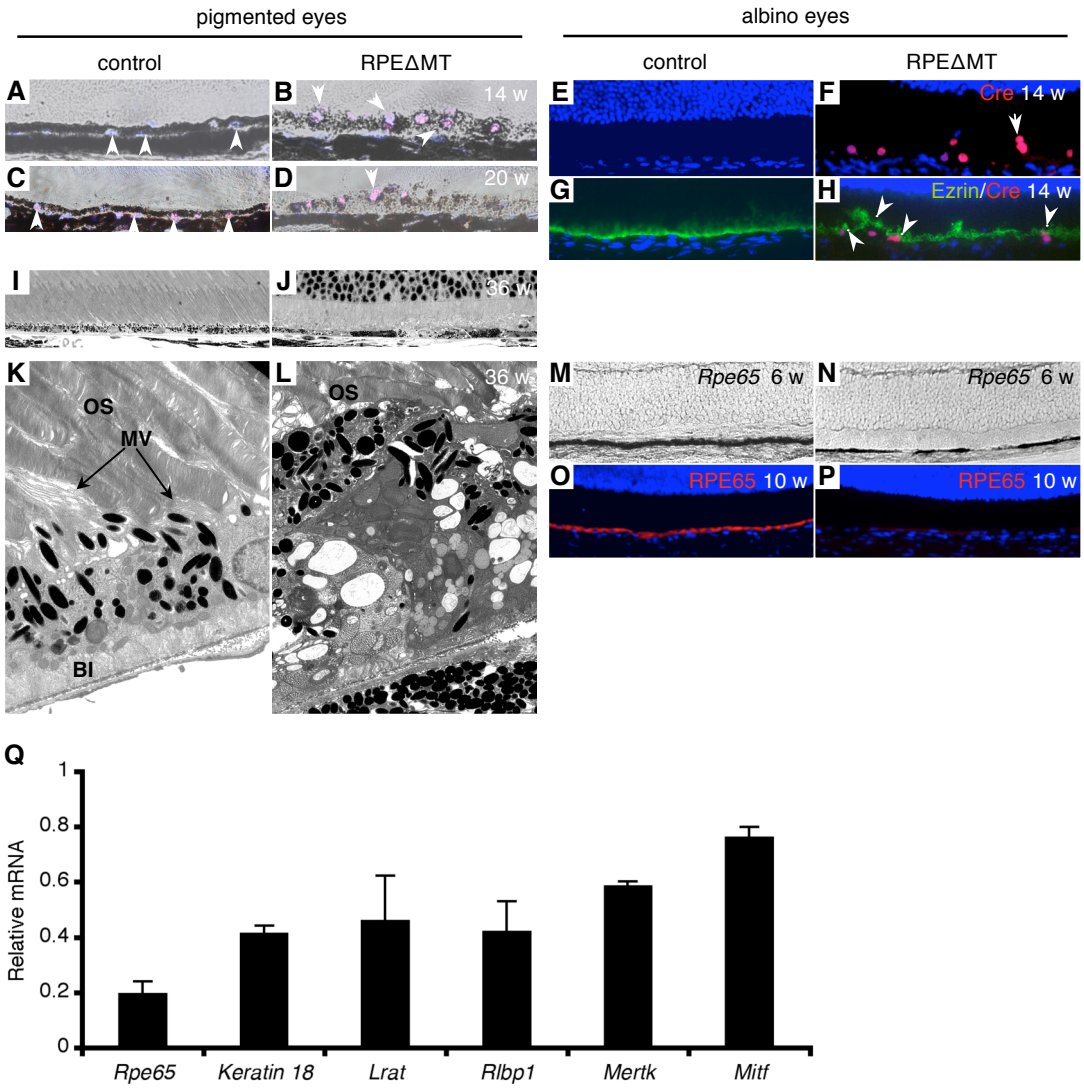

Figure S3. Phenotypic and molecular abnormalities of RPE in RPEΔMT mice. (**A-F**) Cre staining with (**A**-**D**) or without (**E** and **F**) DIC image merged. Cre-expressing cells are thickened (**B and D**) with apical location of nuclei and vertical alignment in the case of binucleate cells (**B, D** and **F**, arrows), whereas control RPE cells have basal localized nuclei (**A** and **C**, arrowheads). Control (**C**) is *Tfam*$^{loxp/WT}$; +/Tg(*BEST1-cre*). Abnormal melanosome distribution is observed in cre-expressing RPE cells at 14 and 20 weeks of age (**B** and **D**). (**G** and **H**) Ezrin (green) is delocalized in cre-expressing cells (red) (**H**, arrowheads), whereas ezrin is only located on the apical side in a control (**G**). (**I** and **J**) Light microscopy detects hypo- and hyper- pigmented areas (**J**) in 36-week-old RPEΔMT mice. (**K** and **L**) Electron micrograph of a pigmented eye reveals disorganized photoreceptor outer segments (OS), RPE thickening, loss of microvilli (MV) and loss of basal infoldings (BI) in RPEΔMT mice (**L**). Loss of *Rpe65* mRNA in RPEΔMT mice is detected by *in situ* hybridization as early as 6 weeks of age (**N**) compared to a control (**M**), and RPE65 protein (red) is diminished at 10 weeks (**P**). (**Q**) Q-PCR detects reduced expression of RPE-characteristic markers in pigmented RPE cells of RPEΔMT mice at 14 weeks, as compared to age-matched controls, with *Rpe65* exhibiting the greatest reduction. Error bars represent Average Deviation (ADEV) from two independent experiments, each of which consisted of RPE cells pooled from six RPEΔMT mice.

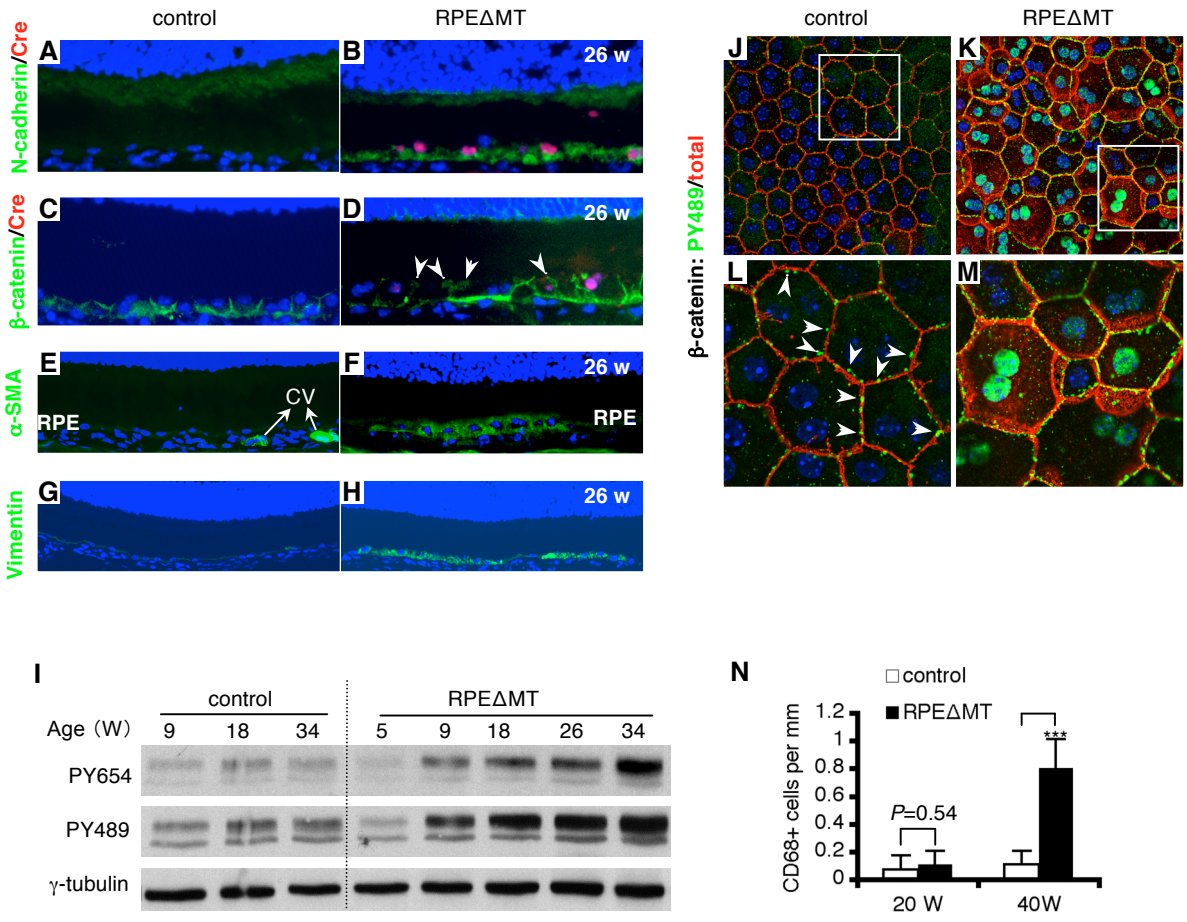

Figure S4. Epithelial to mesenchymal transition-like changes and macrophage invasion in RPEΔMT mice. (**A**-**H**) Cre-expressing cells (red) have increased N-cadherin (**B**, green), and disrupted β-catenin staining at cell junctions (**D**, green; arrowheads denote disruption of β-catenin). Reactivity of α-SMA (**F**, green) and vimentin (**H**) are also increased in RPEΔMT mice. Abbreviation: CV, choroidal vessel. (**I**) Increased tyrosine phosphorylation of β-catenin at residues Y489 and Y654 in eyecups from RPEΔMT mice is evident with age. (**J**-**M**) Co-staining for phosphorylated β-catenin^{PY489} (green) and total β-catenin (red) shows minimal but detectable β-catenin^{PY489} staining in a control (**J** and **L**), mostly located near cell boundaries (**L**, arrowheads). RPEΔMT mice have increased cytoplasmic and nuclear β-catenin^{PY489} at RPE cell junctions at 22 weeks (**K** and **M**). (N) Quantification of CD68-reactive cells in retinal sections indicates invasion by macrophages in RPEΔMT mice by 40 weeks of age.

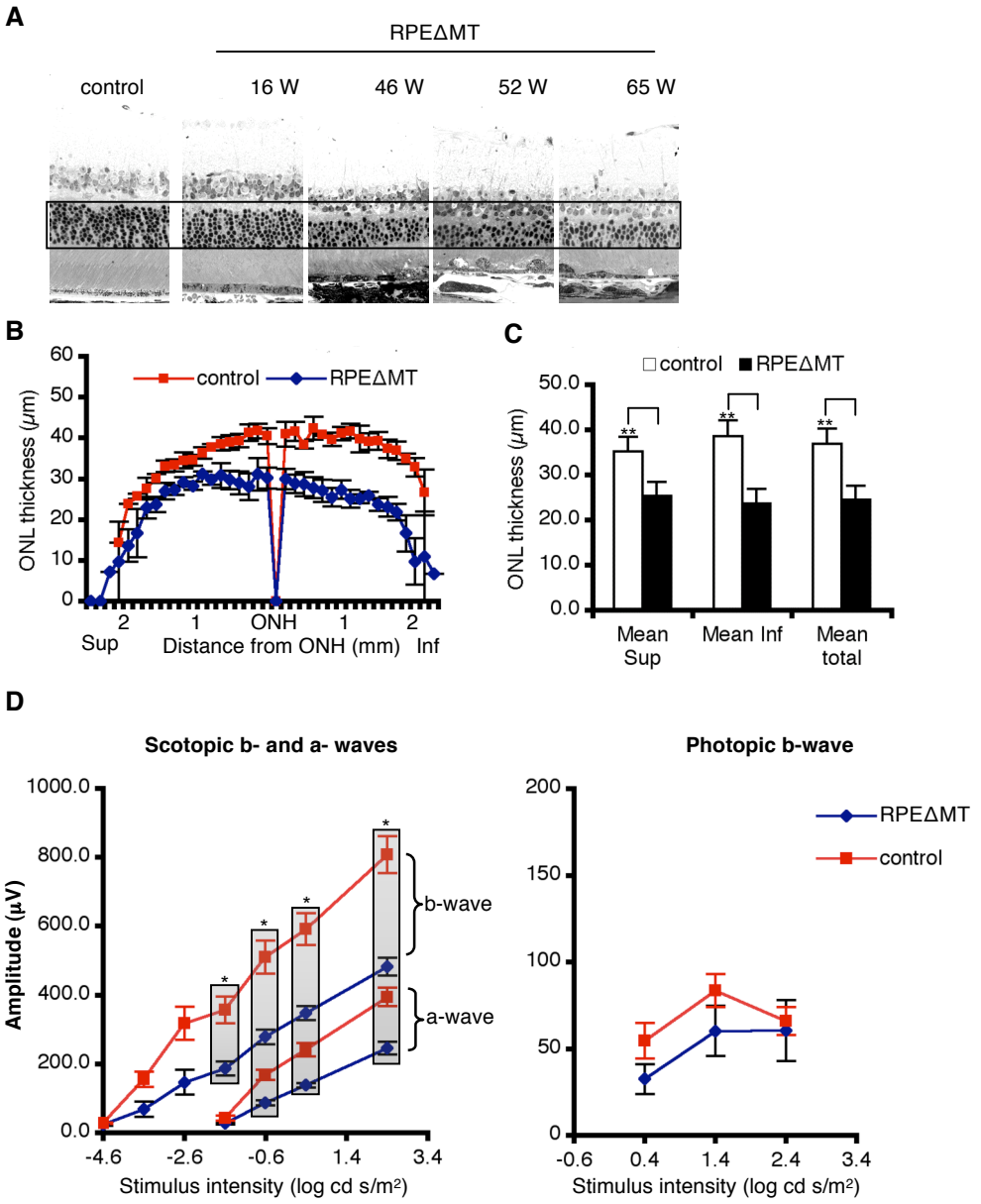

Figure S5. Photoreceptor degeneration in pigmented RPEΔMT mice. (**A**) Light micrographs from posterior retinas show progressive regional loss of photoreceptors as demonstrated by a reduction in the thickness of the outer nuclear layer (ONL) (box). (**B**) Global assessment of ONL thickness in RPEΔMT mice and controls at 52-65 weeks of age. (**C**) Quantification of mean ONL thickness in the same RPEΔMT mice (n = 4) and controls (n = 4) as those measured in **B**. Abbreviations: Sup., superior retina; ONH, optic nerve head; Inf., inferior retina. (**D**) Electroretinography demonstrates a significant reduction in rod responses (scotopic b- and a- waves), and a modest reduction in cone responses (photopic b-wave) in 24-week-old RPEΔMT mice (n=3) compared to age-matched controls (n=4). Data represent mean ± SEM. Note, both RPEΔMT mice and controls were treated with the vehicle used for rapamycin administration (see Methods).

mTOR-Mediated Dedifferentiation of the Retinal Pigment Epithelium Initiates Photoreceptor Degeneration in Mice

Supplemental Figures 6-10

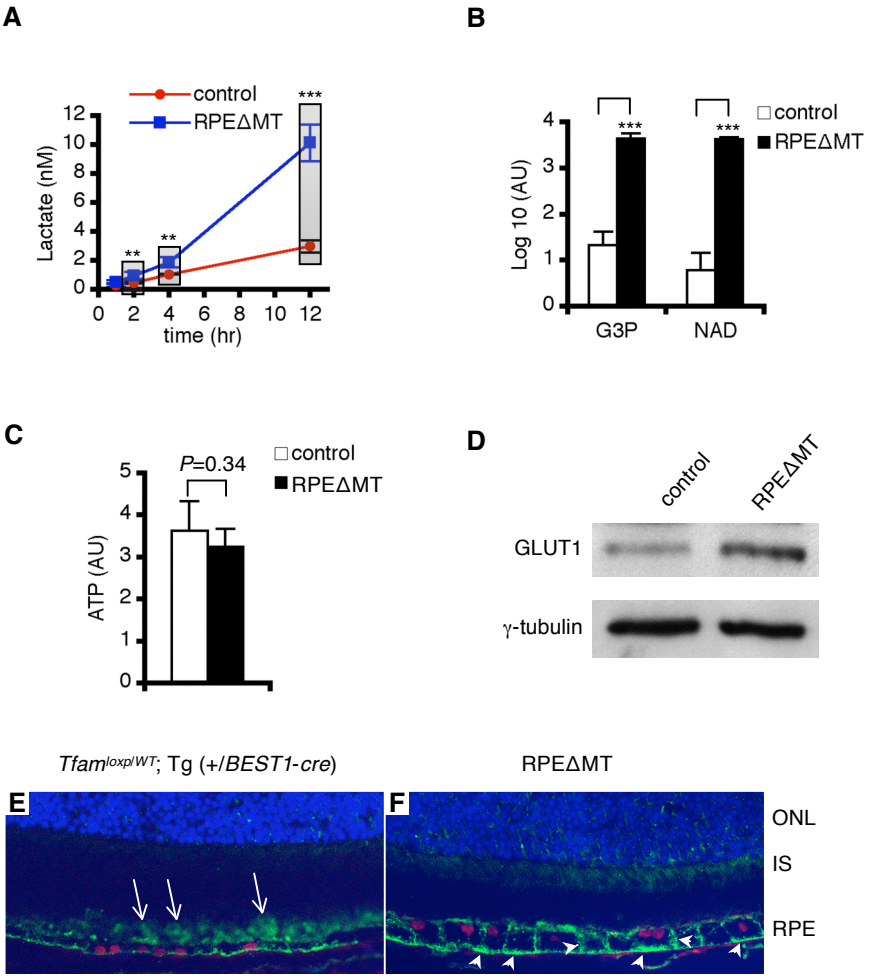

Figure S6. Assessment of glycolysis-related metabolites and protein. (**A**) Lactate secretion is significantly increased in culture media collected at multiple time points from RPEΔMT RPE explants (triplicates). (**B**) Glycerol 3-phosphate (G3P) and NAD are increased several hundred-fold in RPE cells of RPEΔMT mice compared to controls (duplicates). (**C**) ATP levels are similar in RPE cells from RPEΔMT mice and controls (triplicates). AU means arbitrary units. (**D**) Immunoblot detects increased GLUT1 in RPE cells of RPEΔMT mice. (**E** and **F**) Immunostaining for GLUT1 and cre shows RPEΔMT mice have increased reactivity of GLUT1 in the basolateral RPE (**F**, arrowheads) and inner segments (IS) of photoreceptors, and decreased reactivity of GLUT1 at the apical microvilli when compared to a control (**E**, arrows).

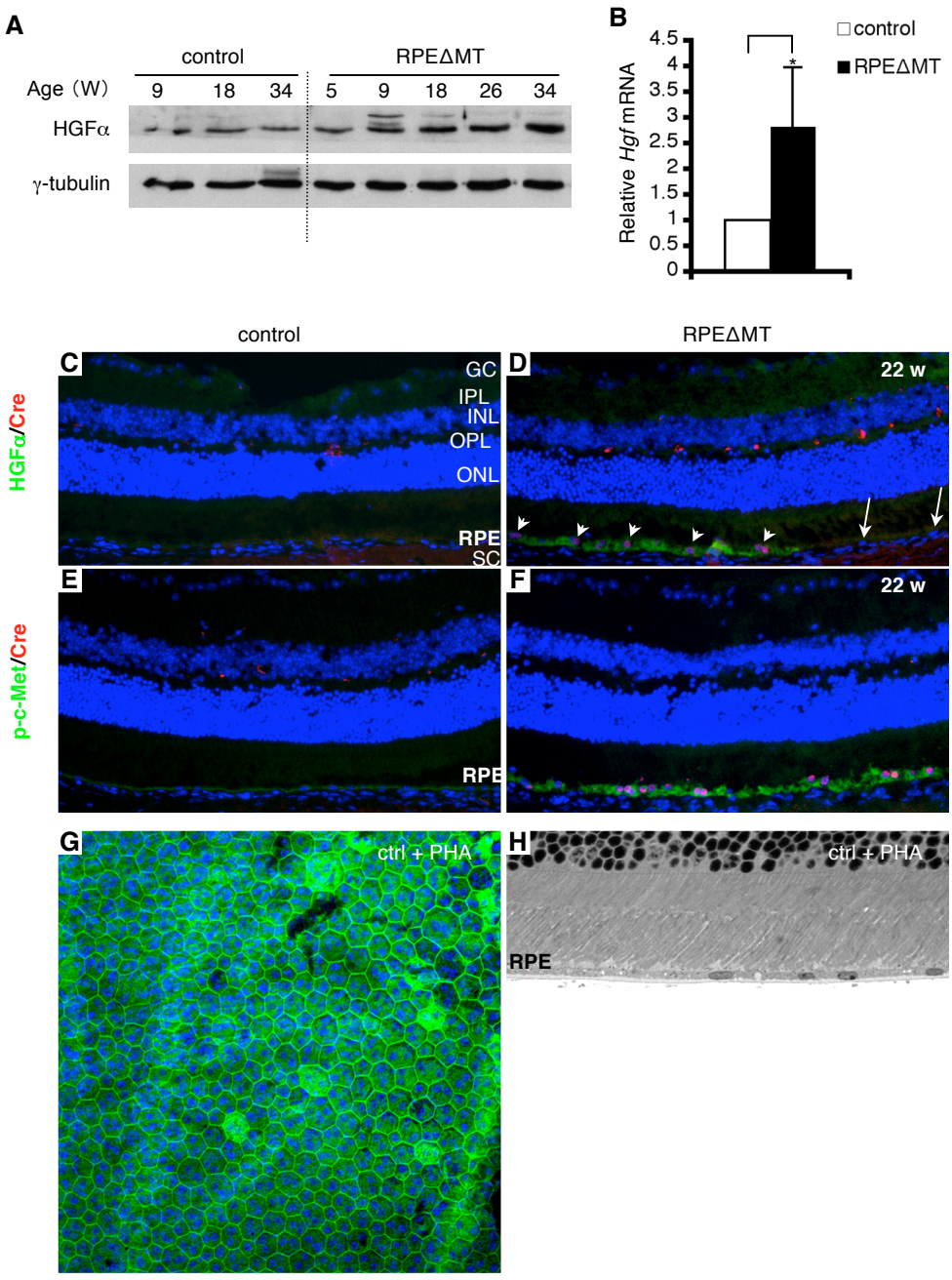

Figure S7. Activation of HGF/c-Met pathway in RPEΔMT RPE. (**A**) Immunoblot detects progressively increased HGF reactivity in eyecups from albino RPEΔMT mice. (**B**) *Hgf* mRNA is increased in eyecups from RPEΔMT mice at 22 weeks of age. Error bars represent STDEV from triplicates. (**C**-**F**) Immunostaining of retinal sections for HGF (green) shows some reactivity in the RPE, IPL and GC layer in a control (**C**). In RPEΔMT mice (**D**), HGF reactivity is significantly increased in cre-expressing RPE cells (purple cells denoted by arrowheads), but not in the cre-negative RPE cells (arrows). P-c-Met$^{Y1234/1235}$ (green) is only detectable in the RPE layer in both controls (**E**) and albino RPEΔMT mice (**F**), and remarkably increased in the latter, correlating with cre-expressing RPE cells (purple). Background red signals arising from the secondary antibody alone were sometimes observed in SC and OPL layer. (**G** and **H**) Evaluation of control mice injected with PHA-665752 by phalloidin staining of a RPE flatmount (**G**, Z-scanning images) and light microscopy (**H**). No abnormalities were observed.

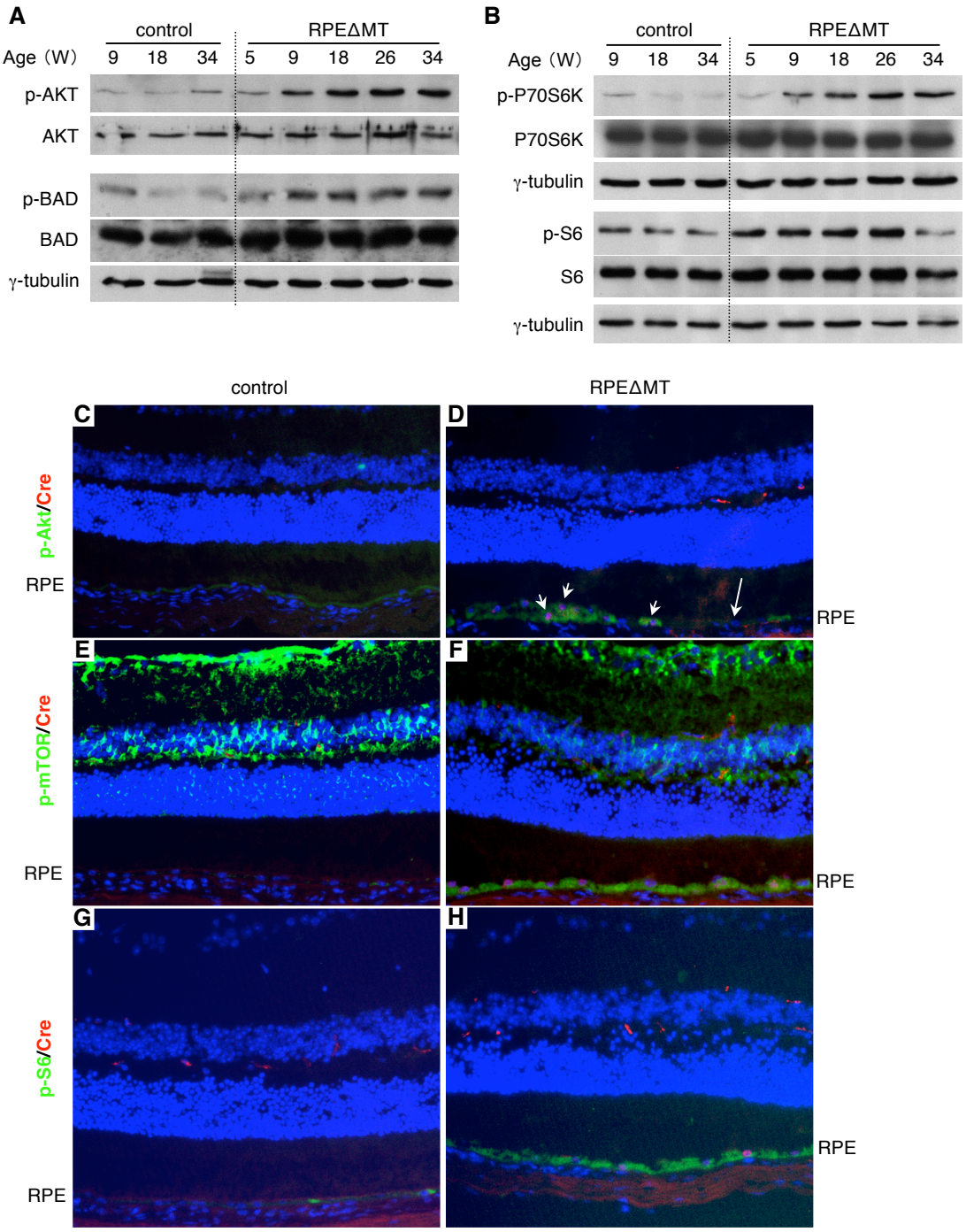

Figure S8. Assessment of PI3K/AKT/mTOR pathway in albino RPEΔMT RPE. (**A** and **B**) Immunoblot detects progressively increased phosphorylation of (**A**) AKT^{Ser473}, BAD^{Ser136}, (**B**) P70SK6^{Thr389} and S6$^{Ser235/236}$ in eyecups of RPEΔMT mice, compared to controls. (**C**-**H**) Immunostaining on retinal sections detects basal reactivity of AKT^{Ser473} (green) in the RPE of a control (**C**). In RPEΔMT mice (**D**), AKT^{Ser473} reactivity is significantly increased in cre-expressing RPE cells (purple cells denoted by short arrows), but not in cre-negative RPE cells (long arrow). Phosphorylated mTOR^{Ser2448} (green) is detectable in multiple retinal layers in both control (**E**) and albino RPEΔMT mice (**F**), but remarkably increased in the RPE of the latter, correlating with cre expression (purple). Reactivity of p-S6$^{Ser235/236}$ is also specifically increased in the RPE of RPEΔMT mice (**H**).

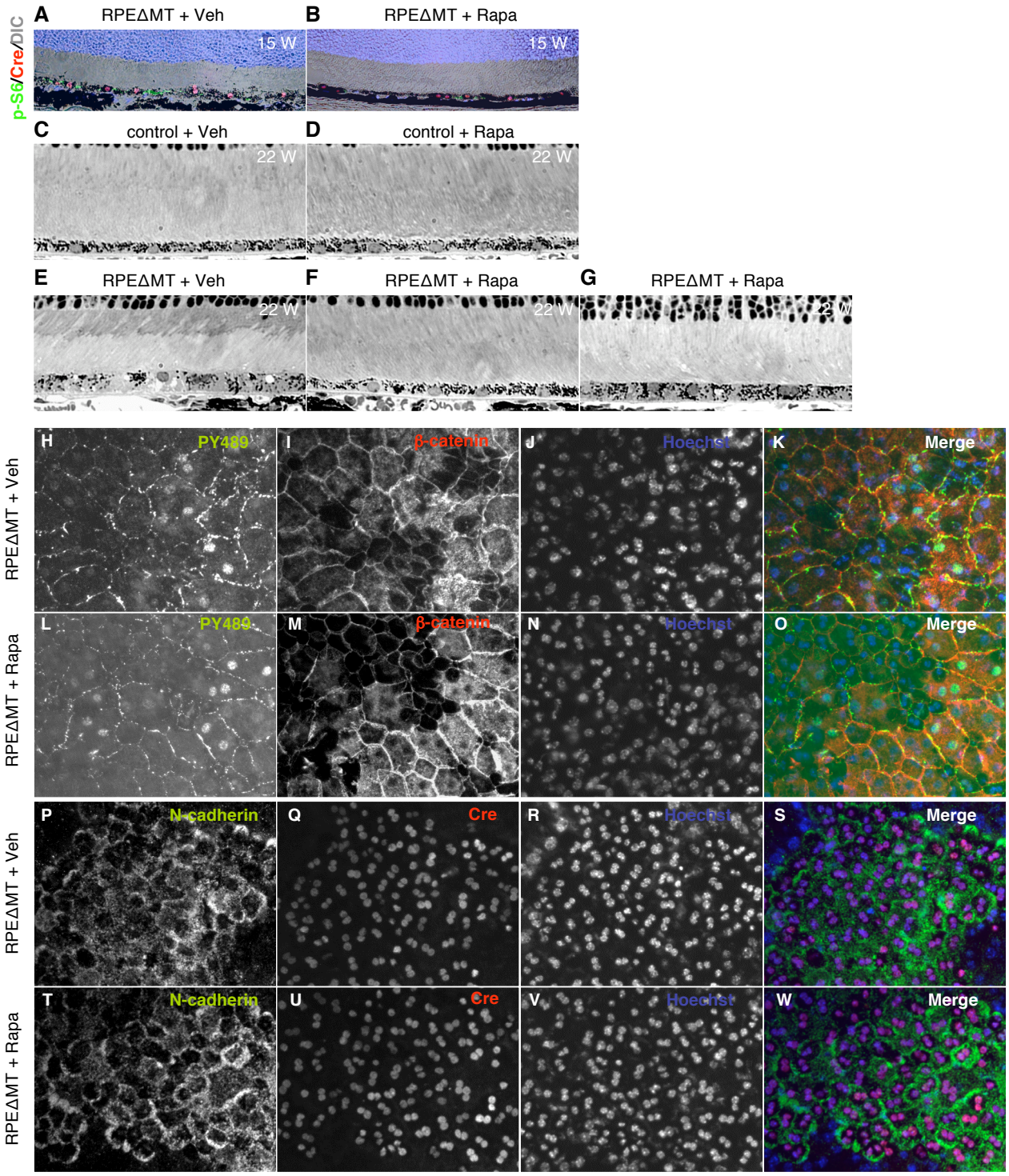

Figure S9. Effect of rapamycin treatment on pigmented RPEΔMT mice and controls. (**A** and **B**) Merged images of immunostaining for p-S6$^{Ser235/236}$ (green) and cre (red), and DIC taken from RPEΔMT mice. Decreased p-S6$^{Ser235/236}$ reactivity in cre-expressing RPE cells as a result of rapamycin treatment (**B**) correlates with normalized melanosome distribution, nuclear alignment and RPE thickness, compared to a vehicle-treated RPEΔMT control (**A**). (**C**-**G**) Light microscopy detects unchanged RPE phenotype in controls treated with rapamycin (**D**) compared to vehicle-treated controls (**C**). While only abnormal RPE cells were observed in 22-week-old RPEΔMT mice treated with vehicle (**E**), RPEΔMT mice treated with rapamycin have normal-appearing RPE cells (**F**) and thickened RPE cells (**G**) in the same retina. (**H**-**W**) Immunostaining of RPE flatmounts shows a similar distribution of p-β-catenin^{Y489} (**H** and **L**), β-catenin (**I** and **M**) and N-cadherin (**P** and **T**) between rapamycin-treated and vehicle-treated RPEΔMT mice.

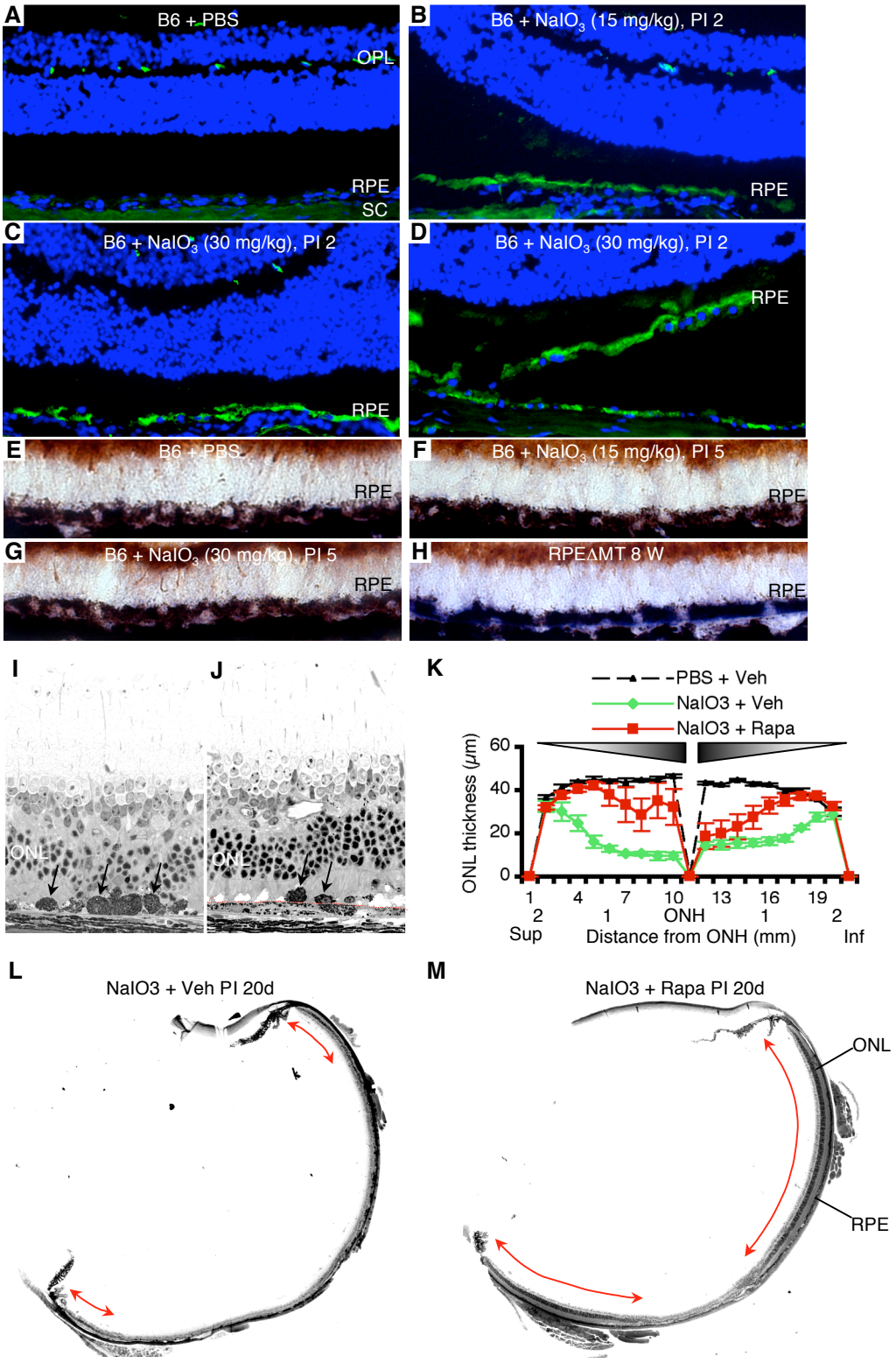

Figure S10. $NaIO_3$-induced RPE oxidative stress in B6 mice and rapamycin reversal of the consequent retinal degeneration. (**A**-**D**) Staining of retinal sections for 8-OHDG, a marker of oxidatively damaged RNA and DNA, shows a dose-dependent increase in reactivity at post-injection (PI) day 2 caused by intravenous injection of $NaIO_3$ (**B**-**D**). Background signals in SC and OPL are due to the secondary antibody. (**E**-**H**) Histochemical co-staining for COX and SDH in sections from pigmented eyes reveals a dark brown stain in the RPE of mice injected with 1X PBS (**E**), 15 mg/kg $NaIO_3$ (**F**) and 30 mg/kg $NaIO_3$ (**G**) at PI 5d. The dark brown color in the RPE is a result of combined COX/SDH activities and endogenous melanin. As a control, 8-week-old pigmented RPEΔMT mice show blue-stained RPE indicative of COX deficiency (**H**). (**I** and **J**) At PI 17d, light microscopy detects substantial atrophic RPE (**I**) and thickened, multilayered RPE (**J**) with numerous cells (arrows) in the subretinal space, delineated in **J** by a dashed red line. (**K**) Quantification of ONL thickness from superior (Sup) to inferior (Inf) retina reveals dramatically degenerated ONL spanning the entire posterior region in $NaIO_3$-injected mice (green curve, n = 6) at PI 17d. Gray scale wedges denote the central to peripheral gradient of ONL degeneration caused by $NaIO_3$. The resulting ONL defect is significantly rescued by rapamycin (red curve, n = 6) in large areas of the retina. PBS and vehicle-treated mice serve as controls (black curve, n = 4). (**L** and **M**) Representative retinal sections from vehicle-treated (**L**) and rapamycin-treated (**M**) $NaIO_3$-injected mice at PI 20d illustrate the remarkable rescue effect of rapamycin on retinal histology. The double-headed red arrows denote histologically normal retina.

mTOR-Mediated Dedifferentiation of the Retinal Pigment Epithelium Initiates Photoreceptor Degeneration in Mice

Supplemental Methods:

COX and SDH enzyme histochemistry, senescence associated β-galactosidase histochemistry, TUNEL and oil red O staining. COX and SDH enzyme histochemistry was done as previously described (1). A senescence-associated β-galactosidase staining kit was purchased from Cell Signaling Technology. A TUNEL staining kit was purchased from Roche Applied Science. Oil red O solution was purchased from Millipore. Procedures were performed according to the manufacturers' instructions.

Immunoblot. Protein lysates were prepared as described previously (2) from eyecups and isolated RPE cells. Total protein for each sample was quantified with a BCA kit (Roche Applied Science). An equal amount of protein from each sample was separated by 12% or 4-16% gradient SDS-PAGE. Protein transfer and chemiluminescence detection was done as described previously (3). For protein quantification, the intensity of bands was quantified by ImageJ and normalized by γ-tubulin.

Histology, electroretinography and funduscopy. Electroretinography and the preparation of plastic embedded sections for light microscopy were done as described elsewhere (4). For electron microscopy, ultrathin sections (100 nm) were cut on a Leica Ultracut microtome (Leica Microsystems), collected on 200 mesh copper grids, stained with uranium and lead salts, and viewed on a Zeiss 910 transmission electron microscope (Zeiss Inc.). Living funduscopy of mice was performed with a MICRON II (Phoenix Research Laboratories).

Liquid chromatography-mass spectrometry (LC-MS) and metabolite analysis. Isolated RPE cells were subjected to LC-MS analysis to quantify metabolites. RPE cells were first frozen on dry

ice. Pre-boiled extraction buffer containing 75% methanol and 1 μM 3'Br-cAMP (loading control) was poured on cells. After a brief vortex, cells were boiled for 3 minutes and spun down for 10 minutes at 4°C in a microfuge. The supernatant was transferred to a glass vial and loaded onto a Waters Acquity UPLC-coupled Thermo TSQ Vantage Triple Quad mass spectrometer. Three injections per sample were used as replicates. UPLC Amide columns (Thermo Scientific). were used. The residual cell pellet (containing proteins that are insoluble in methanol) was resuspended in protein lysis buffer, and the protein concentration was quantified by BCA assay as before. The relative mass abundance of each metabolite was determined in LCquan V2.6 (Thermo Scientific) and normalized by the 3'Br-cAMP mass peaks. Relative values of NAD and G3P were further normalized by internal succinate because this metabolite was not noticeably changed in RPEΔMT mice, which is in agreement with the preserved SDH function as previously described (5). Relative ATP values were normalized by protein amount. Lactate secretion was measured in culture medium of RPE explant after 12 hours of incubation. RPE explant was prepared as described previously (6) and cultured in DMEM supplemented with 0.45% glucose, 10% FBS, 2 mM glutamine, 50 μg/ml uridine, and 1 mM pyruvate, as described (7).

Quantification. For cre-expressing and total RPE cell quantification, cells were counted on RPE flatmounts that were co-immunostained for cre and junctional markers (phalloidin or ZO1). Eight random areas (225 μM X 225 μM) from each eye were selected for counting. For Brdu reactive cells and macrophage/microglia quantification, cells were counted on cross sections stained with Brdu or CD68 antibody, respectively. Three sections (6 X 450 μM length of retina) from each eye were counted. For maximal mitochondrial area measurement, 1-2 electron micrographs with "maximal" numbers of mitochondria were selected from each animal. RPEΔMT mice (22 to 36 weeks of age) and age-matched controls were compared. Outer nuclear layer (ONL) thickness under light microscopy was used as a measure of photoreceptor

number, with quantification performed as described previously (4). RPE thickness and cone numbers were also quantified under light microscopy. One or two entire retinal cross sections that included the optic nerve head (ONH) were selected from each mouse for quantification (20 measurements per retina). Maximal and minimal RPE thickness were measured on 1000X light micrographs taken from selected representative areas. For quantification of cellular protein content, total protein amount of isolated RPE cells (from 3 to 6 mice) was measured by BCA assay and then divided by cell number.

Supplementary Table 1. Primers for *in situ* hybridization and expression studies.

Gene	Forward primer (5' -> 3')	Reverse primer (5' -> 3')
For in situ hybridization probes		
Rpe65	CTAGTGAATTCAATTTGGCACCTGTGCTTTC	ACTTAGAAGCTTGAGGCCCTGAAAAGAGAACC
Mt-Co1	CTAGTGAATTCCCAGATATAGCATTCCCACGA	ACTTAGAAGCTTAAGTGGGCTTTTGCTCATGT
For quantitative PCR *Mitochondria-related genes (nuclear and mitochondrial encoded)*		
Mt-Atp6	CACCAAAAGGACGAACATGA	GGTAGCTGTTGGTGGGCTAA
Mt-ND4	CCCTAATCGGTTCTATTCCAC	TGGGTCTAGAATAATGGAGATGC
Mt-ND6	TCCACCCATGACTACCATCA	TGTGTAGGAATGCTAGGTGTGG
Tfam	CCTTCGATTTTCCACAGAACA	TTCCAAGCCTCATTTACAAGC
Aif	CCGAGTACCCTGAGAAGGAG	GCCAGCCTACTCTCAAATGC
RPE characteristic markers		
Rpe65	CAGGGCTCTTTGAAGTTGGA	CAGTGGCACCATTGACAGAA
Rlbp1	GATCATGGTCCTGTCTTTGG	ATAAGCACGACCCACATCG
Krt18	CGAGGCACTCAAGGAAGAAC	CTTGGTGGTGACAACTGTGG
Lrat	TCACCTAGACGGGACTCTCAA	TAATCCCAAGACAGCCGAAG
Mertk	GTTCAGCATAGCCAGTGTGC	TTTTTCATTAACACGGCTGCT
Mitf	ACGACCGCATTAAGGAGCTA	GGTGGATGGGATAAGGGAAA
Growth factors		
Hgf	AACAACTGCGGGTTGTAAATG	CAGGTCGAGCAAGCTTCAGT
Tgf-B2	CGAGGAGTACTACGCCAAGG	GCAGGGGCAGTGTAAACTTATT
Egf	TTAAGCCGAGACCGGAAGTA	ACCATTGTCAGGCGATGAAC
Igf1 (206)	AGCTGGACCAGAGACCCTTT	CTTCAGTGGGGCACAGTACA
Fgf2 (204)	ATGTTGGTGACCACAAGCTG	ACTGCCCAGTTCGTTTCAGT
Housekeeping genes		
Eef1e1	GCAGAAGAAAAGGCAATGGT	AGGCCGTAGTACAGCAGGAT
γ-tubulin	ATCTACCTGTCGGAGCATGG	GGAACACAGAGTATGTCTGCACT

All primers were designed according the Ensembl genome database at <http://uswest.ensembl.org/index.html>.
For genes with multiple transcripts, the relevant transcript number is in parenthesis, following the gene name.

Supplementary Table 2. Antibodies used in this study.

Antigen	Host	Immunoblot	Immunostaining	Supplier
General				
Cre	mouse	1:1500	1:400, IF	Millipore
RPE65	mouse	1:3500	1:250, IF	Millipore
Keratin 18	mouse	1: 2000	no	Abcam
MITF	rabbit	1:1500	no	Abcam
RLBP1	rabbit	1:40000	no	non comercial
MERTK	rabbit	1:5000	no	non comercial
LRAT	rabbit	1:800	no	non comercial
Na/K ATPase	mouse	no	1:150, IF	Millipore
Brdu	rat	no	1:500, IF	Accurate
Ki67	rabbit	no	1:500, IF	Abcam
F4/80	rat	no	1:50, IF	Abcam
CD68	rat	no	1:150, IF	Abcam
macrophage	rat	no	1:50, IF	Abcam
8-OHDG	mouse	no	1:500, IF	Alpha
N-cadherin	rabbit	1:1500	no	Cell Signaling
N-cadherin	rabbit	no	1:150, IF	Abcam
β-catenin	rabbit	1:1500	1:150, IF	Cell Signaling
β-catenin^{Tyr489}	mouse	1:300	1:100, IF	DSHB
β-catenin^{Tyr654}	mouse	1:300	no	DSHB
ZO1	rabbit	no	1:150, IF	Invitrogen
SMA	mouse	no	1:50, ABC	Millipore
Vimentin	rabbit	no	1:150, ABC	Abcam
B-Tubulin	mouse	no	1:100, IF	DSHB
M-opsin	rabbit	no	1:200, IF	Millipore
GLUT1	rabbit	1:5000	no	Abcam
AKT^{Ser473}	rabbit	1:1200	1:200, ABC	Cell Signaling
AKT	rabbit	1:1200	no	Cell Signaling
P85^{Tyr458}	rabbit	1:1200	no	Cell Signaling
P85	rabbit	1:1200	no	Cell Signaling
GSK-3b^{Ser9}	rabbit	1:1200	no	Cell Signaling
GSK-3b	rabbit	1:3000	no	Cell Signaling
BAD^{Ser136}	rabbit	1:1000	no	Cell Signaling
BAD	rabbit	1:3000	no	Cell Signaling
TSC2^{Thr1462}	rabbit	1:1000	no	Cell Signaling
TSC2	rabbit	1:1000	no	Cell Signaling
mTOR^{Ser2448}	rabbit	1:800	no	Millipore
mTOR^{Ser2448}	rabbit	no	1:150, ABC	Cell Signaling
mTOR	rabbit	1:2000	no	Cell Signaling
P70SK6^{Thr389}	rabbit	1:1500	no	Cell Signaling
P70SK6	rabbit	1:2000	no	Cell Signaling
S6$^{Ser235/236}$	rabbit	1:2000	1:150, ABC	Cell Signaling
S6	rabbit	1:2000	no	Cell Signaling

Detection of apoptosis and autophagy				
Cleaved caspase 9	rabbit	1:1000	1:50, IF	Cell Signaling
Cleaved caspase 3	rabbit	1:1000	1:400, IF	Cell Signaling
Cleaved caspase 7	rabbit	1:1000	1:100, IF	Cell Signaling
Caspase 9	rabbit	1:1000	no	Cell Signaling
Caspase 3	rabbit	1:1000	no	Cell Signaling
Caspase 7	rabbit	1:1000	no	Cell Signaling
AIF	rabbit	1:3000	1:300, IF	Millipore
AMPKα^{Tyr172}	rabbit	1:1000	no	Cell Signaling
AMPKα	rabbit	1:1000	no	Cell Signaling
LC3B	rabbit	1:1000	1:100, IF	Cell Signaling
Atg12-Atg5	rabbit	1:1000	1:100, IF	Cell Signaling
Lamp1	mouse	1:300	1:20, IF	DSHB
Lamp2	mouse	1:300	1:20, IF	DSHB
Detection of growth factor pathways				
HGFα	rabbit	1:300	1:50, IF	SCBT
c-Met$^{Tyr1234/1235}$	rabbit	1:1200	1:300, ABC	Cell Signaling
c-Met	mouse	1:1200	no	Cell Signaling
TGF-β	rabbit	1:1200	1:50, IF	Cell Signaling
Smad2$^{Ser456/457}$	rabbit	1:1200	1:50, IF	Cell Signaling
Smad2	rabbit	1:1200	no	Cell Signaling
BMP4	rabbit	1:1200	no	Millipore
Smad1/5$^{Ser463/465}$	rabbit	1:1200	no	Cell Signaling
Smad5	rabbit	1:1200	no	Cell Signaling
VEGF	rabbit	1:2000	1:200, IF	Abcam
VEGFR2^{Tyr1054}	rabbit	1:2000	no	Abcam
VEGFR2	rabbit	1:1000	no	Millipore
EGFR^{Tyr845}	rabbit	1:1200	no	Cell Signaling
EGFR	rabbit	1:1200	no	Cell Signaling
IGF-IR$^{Tyr1135/1136}$	rabbit	1:1200	no	Cell Signaling
IGF-IR	rabbit	1:1200	no	Cell Signaling
bFGF	mouse	1:200	no	SCBT

Note: Antibodies directed against RLBP1 (8) and MERTK (9) have been described. The RLBP1 antibody was a kind gift from Dr. Jack Saari (Department of Ophthalmology, University of Washington, Seattle, Washington 98185). A rabbit polyclonal antibody against LRAT was generated by immunizing with a peptide corresponding to residues 27 to 46 of the mouse LRAT protein (D. Bok, unpublished). For immunostaining, IF denotes a two-step staining process in which a fluorescently-labeled secondary antibody was applied; ABC denotes the use of the Avidin-Biotinylated Complex system, as recommended by the commercial supplier. In this procedure, a biotin and avidin blocking step was performed, in addition to the normal blocking procedure described in the Methods section. Biotinylated secondary antibodies were applied, followed by fluorescently-labeled strepavidin (Vector laboratories). Full names for commercial suppliers: Cell Signaling Technology; Millipore; Abcam Inc.; Accurate Chemical Scientific Corporation; DSHB denotes Developmental Studies Hybridoma Bank at University of Iowa; SCBT denotes Santa Cruz BioTechnology, Inc,; Alpha denotes Alpha Diagnostic International Inc,.

References for Supplemental Methods:

1. Seligman AM, Karnovsky MJ, Wasserkrug HL, and Hanker JS. Nondroplet ultrastructural demonstration of cytochrome oxidase activity with a polymerizing osmiophilic reagent, diaminobenzidine (DAB). *J Cell Biol*. 1968;38(1):1-14.
2. Strick DJ, Feng W, and Vollrath D. Mertk drives myosin II redistribution during retinal pigment epithelial phagocytosis. *Invest Ophthalmol Vis Sci*. 2009;50(5):2427-2435.
3. Liu Y, and Vollrath D. Reversal of mutant myocilin non-secretion and cell killing: implications for glaucoma. *Hum Mol Genet*. 2004;13(11):1193-1204.
4. Duncan JL, LaVail MM, Yasumura D, Matthes MT, Yang H, Trautmann N, Chappelow AV, Feng W, Earp HS, Matsushima GK, et al. An RCS-like retinal dystrophy phenotype in mer knockout mice. *Invest Ophthalmol Vis Sci*. 2003;44(2):826-838.
5. Larsson NG, Wang J, Wilhelmsson H, Oldfors A, Rustin P, Lewandoski M, Barsh GS, and Clayton DA. Mitochondrial transcription factor A is necessary for mtDNA maintenance and embryogenesis in mice. *Nat Genet*. 1998;18(3):231-236.
6. Rattner A, Toulabi L, Williams J, Yu H, and Nathans J. The genomic response of the retinal pigment epithelium to light damage and retinal detachment. *J Neurosci*. 2008;28(39):9880-9889.
7. Pelicano H, Xu RH, Du M, Feng L, Sasaki R, Carew JS, Hu Y, Ramdas L, Hu L, Keating MJ, et al. Mitochondrial respiration defects in cancer cells cause activation of Akt survival pathway through a redox-mediated mechanism. *J Cell Biol*. 2006;175(6):913-923.
8. Saari JC, Nawrot M, Kennedy BN, Garwin GG, Hurley JB, Huang J, Possin DE, and Crabb JW. Visual cycle impairment in cellular retinaldehyde binding protein (CRALBP) knockout mice results in delayed dark adaptation. *Neuron*. 2001;29(3):739-748.
9. Feng W, Yasumura D, Matthes MT, LaVail MM, and Vollrath D. Mertk triggers uptake of photoreceptor outer segments during phagocytosis by cultured retinal pigment epithelial cells. *J Biol Chem*. 2002;277(19):17016-17022.